

ARTICLES

Chromosomally unstable mouse tumours have genomic alterations similar to diverse human cancers

Richard S. Maser^{1*}, Bhudipa Choudhury^{4*}, Peter J. Campbell^{4*}, Bin Feng^{2*}, Kwok-Kin Wong¹, Alexei Protopopov², Jennifer O'Neil³, Alejandro Gutierrez^{3,5}, Elena Ivanova², Ilana Perna², Eric Lin⁶, Vidya Mani¹, Shan Jiang¹, Kate McNamara¹, Sara Zaghlul¹, Sarah Edkins⁴, Claire Stevens⁴, Cameron Brennan⁷, Eric S. Martin¹, Ruprecht Wiedemeyer¹, Omar Kabbarah¹, Cristina Nogueira¹, Gavin Histén⁸, Jon Aster⁸, Marc Mansour¹¹, Veronique Duke¹¹, Letizia Foroni¹¹, Adele K. Fielding¹¹, Anthony H. Goldstone¹², Jacob M. Rowe¹³, Yaoqi A. Wang^{1,2}, A. Thomas Look³, Michael R. Stratton⁴, Lynda Chin^{1,2,9}, P. Andrew Futreal⁴ & Ronald A. DePinho^{1,2,10}

Highly rearranged and mutated cancer genomes present major challenges in the identification of pathogenetic events driving the neoplastic transformation process. Here we engineered lymphoma-prone mice with chromosomal instability to assess the usefulness of mouse models in cancer gene discovery and the extent of cross-species overlap in cancer-associated copy number aberrations. Along with targeted re-sequencing, our comparative oncogenomic studies identified *FBXW7* and *PTEN* to be commonly deleted both in murine lymphomas and in human T-cell acute lymphoblastic leukaemia/lymphoma (T-ALL). The murine cancers acquire widespread recurrent amplifications and deletions targeting loci syntenic to those not only in human T-ALL but also in diverse human haematopoietic, mesenchymal and epithelial tumours. These results indicate that murine and human tumours experience common biological processes driven by orthologous genetic events in their malignant evolution. The highly concordant nature of genomic events encourages the use of genomically unstable murine cancer models in the discovery of biological driver events in the human oncogenome.

An increasing compendium of tumour genes underpins the development of effective, targeted therapeutic agents for cancer. This model now influences all aspects of cancer research, motivating intensive efforts in cancer gene discovery. Array-based comparative genome hybridization (array-CGH) has uncovered highly re-arranged human cancer genomes harbouring many recurrent copy number alterations (CNAs)¹. Targeted re-sequencing of human cancers has uncovered pathogenetic mutations in genes such as *BRAF* in melanoma² and *NOTCH1* in T-cell acute lymphoblastic leukaemias/lymphomas (T-ALL)³. Nonetheless, identifying true cancer genes, that is, differentiating 'causal' genomic events from bystander 'genomic noise', remains challenging.

A growing body of evidence, including cross-species preservation of oncogene transcriptional signatures⁴ and synteny of tumour-associated CNAs⁵⁻⁹, indicates that mouse models of human cancer can serve as biologically relevant filters for complex human oncogenomes. More recent high-resolution genomics-based studies have proven that such cross-species comparisons enable the efficient identification of new oncogenes in human cancers^{10,11}, and re-sequencing of key genes in murine cancer models reveals conservation of somatic signature mutational events¹². However, a limitation of mouse cancer models for comparative oncogenomics is the relatively benign cytogenetic profiles of most genetically engineered murine cancers^{8,10,11,13}. On the other

hand, murine cancer genomes can be destabilized experimentally, to simulate the rampant chromosomal instability of human cancers, including those with telomere dysfunction, impaired DNA damage checkpoints such as *Atm*, dominant *Trp53* mutant alleles, and defective DNA repair¹⁴⁻²¹. These 'instability models' of cancer, coupled with high-resolution genomic technologies, hold the potential to provide highly informative systems for comparative oncogenomics.

In this study, we generated a murine lymphoma model that combines the genome-destabilizing impact of *Atm* deficiency and telomere dysfunction to effect T lymphomagenesis in a *Trp53*-dependent manner. We applied multiple genome analysis technologies to identify cancer-associated alterations shared between our mouse model and human cancers. These systematic cross-species comparisons uncovered many syntenic CNAs, not only in lymphomas of the T-cell lineage, but also in other human tumour types, emphasizing the common genetic and biological events in mouse models of cancer. Re-sequencing of candidate genes in syntenic CNAs readily identified *FBXW7* and *PTEN* as commonly mutated genes in human T-ALL.

Results

Generation of murine T-cell lymphomas with highly complex genomes.

Nearly all *Atm*^{-/-} mice develop thymic lymphomas²² with moderate levels of aneuploidy and recurrent chromosomal rearrangements²³. In

¹Department of Medical Oncology, ²Center for Applied Cancer Science of the Belfer Institute for Innovative Cancer Science, ³Department of Pediatric Oncology Dana Farber Cancer Institute, Boston, Massachusetts 02115, USA. ⁴Cancer Genome Project, Wellcome Trust Sanger Institute, Hinxton, Cambridge CB10 1SA, UK. ⁵Division of Hematology, Children's Hospital, Boston, Massachusetts 02115, USA. ⁶Agilent Technologies, Palo Alto, California 94304, USA. ⁷Department of Neurosurgery, Memorial Sloan Kettering Cancer Center, New York, New York 10021, USA. ⁸Department of Pathology, ⁹Department of Dermatology, ¹⁰Department of Genetics and Medicine, Harvard Medical School, Boston, Massachusetts 02115, USA. ¹¹Royal Free and University College Medical School, London NW3 2PF, UK. ¹²University College London Hospitals, London NW1 2BU, UK. ¹³Rambam Medical Center and Technion, Haifa 31096, Israel.

*These authors contributed equally to this work.

Terc^{-/-} *Atm*^{-/-} mice, telomere dysfunction suppresses lymphoma development, which may relate in part to Trp53 activation^{20,21} and/or altered chromosomal dynamics²⁴. To address this directly, we intercrossed *Terc*, *Atm* and *Trp53* mutant mice to generate various genotypic combinations from this 'triple'-mutant colony (hereafter designated as 'TKO' for all genotypes) and found that telomere dysfunction (that is, third (G₃) and fourth (G₄) generation *Terc*^{-/-}; ref. 21) *Trp53*^{+/-} or *Trp53*^{-/-} TKO mice developed lymphoma with shorter latency and higher penetrance relative to *Trp53*^{+/+} TKO animals (Fig. 1a). Moreover, lymphomas from *Trp53*^{+/-} TKO mice showed reduction to homozygosity in 14/15 specimens examined (Fig. 1b), indicating strong genetic pressure to inactivate Trp53 during lymphomagenesis. These TKO tumours resembled those from conventional *Atm*^{-/-} mice with effacement of thymic architecture by CD4⁺/CD8⁺ (less commonly CD4⁻/CD8⁻ or mixed single/double positive) lymphoma cells (Fig. 1c, data not shown). Together, these observations strongly suggest that an *Atm*-independent *Trp53*-dependent telomere checkpoint constrains lymphoma development.

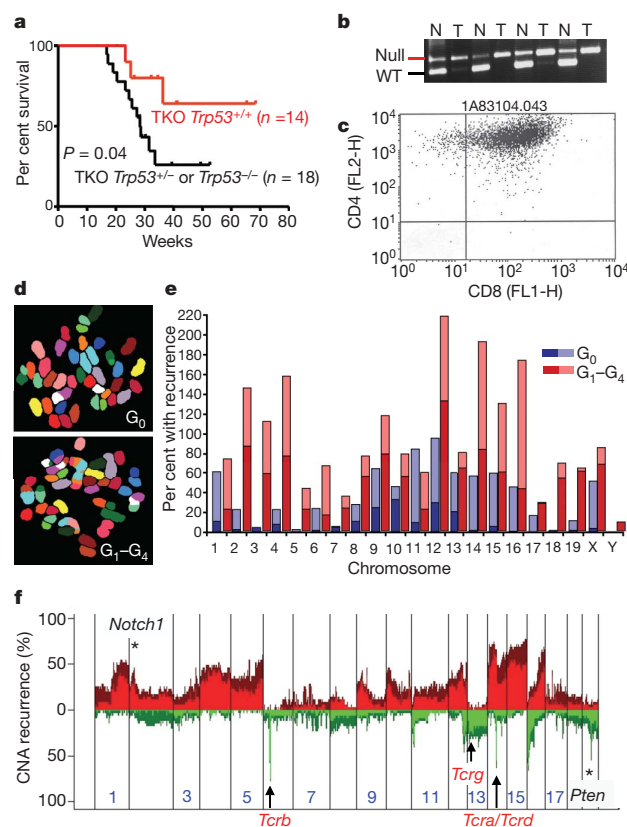


Figure 1 | The TKO model. **a**, Kaplan–Meier curve of thymic lymphoma-free survival for G₃–G₄ TKO mice with varying *Trp53* dosage. **b**, *Trp53* loss of heterozygosity assessed by PCR. N, normal; T, tumour. **c**, Representative FACS profile of a TKO tumour with CD4 and CD8 cell surface marker antibodies. **d**, Representative SKY images from metaphase spreads from G₀ (upper panel) and G₁–G₄ (lower panel) lymphomas. **e**, Quantification of cytogenetic aberrations (recurrences) detected by SKY in G₀ (blue) and G₁–G₄ (red) thymic lymphomas. Darker portion of column indicates proportion of non-reciprocal translocations; lighter portion indicates dicentric/robertsonian-like rearrangements. **f**, Recurrence plot of CNAs defined by array-CGH for 35 TKO lymphomas. The x axis shows the physical location of each chromosome. The percentage of tumours harbouring gains (dark red, log₂ ≥ 0.3), amplifications (bright red, log₂ ≥ 0.6), losses (green, log₂ ≤ -0.3), and deletions (dark green, log₂ ≤ -0.6) for each locus is depicted. Locations of physiologically relevant CNAs at *Tcrb*, *Tcra/Tcrd* and *Tcrg* (arrows), and *Notch1* and *Pten* (asterisks) are indicated.

We undertook spectral karyotype (SKY) analyses to quantify chromosomal rearrangements in nine telomere-deficient (G₁–G₄ *Terc*^{-/-}) and 9 telomere-intact (G₀ *Terc*^{+/+} or *Terc*^{+/-}) TKO lymphomas (Fig. 1d; Supplementary Fig. 1; Supplementary Table 1). Relative to G₀ tumours, G₁–G₄ TKO lymphomas showed a greater frequency of chromosome structural aberrations (0.34 versus 0.09 per chromosome, respectively, *P* < 0.0001, *t*-test), including multicentric chromosomes, non-reciprocal translocations, and p–p, p–q and q–q chromosome arm fusions involving homologous and/or non-homologous chromosomes. Several chromosomes (specifically, 2, 6, 8, 14, 15, 16, 17 and 19) were involved in significantly more dicentric and robertsonian-like rearrangements in G₁–G₄ relative to G₀ TKO tumours (*P* < 0.05; *t*-test; Fig. 1e), suggesting that these events provide adaptive mechanisms to tolerate telomere dysfunction and/or have causal roles in lymphoma development.

TKO tumours acquire genomic lesions syntenic to those in human T-ALL. In the mouse, cancer-associated chromosomal rearrangements of the types described above are by-products of breakage–fusion–bridge cycles associated with telomere dysfunction and defective Trp53 function¹⁴, and similar events can generate amplifications or deletions at the translocation site in human cells²⁵. These processes, together with biological selection, drive emergence of clonal CNAs targeting cancer-relevant genes in the mouse^{6,15}. We therefore compiled high-resolution genome-wide array-CGH profiles of 35 TKO tumours (Supplementary Table 1) and 26 human T-ALL cell lines and tumours (Supplementary Table 2) for comparison. TKO profiles revealed marked genome complexity with all chromosomes exhibiting regional and focal recurrent CNAs (Fig. 1f), some of which were observed in >40% of samples (for example, amplicons targeting distinct regions on mouse chromosomes 1, 2, 3, 4, 5, 9, 10, 12, 14, 15, 16, and 17; and deletions on 6, 11, 12, 13, 14, 16 and 19), corresponding well with rearrangements detected by SKY.

In addition to recurrent physiological deletions of T-cell receptor (*Tcr*) loci (Fig. 1f, arrows; Supplementary Fig. 2) as expected for T-cell derived tumours, we observed pathogenetically relevant recurrent genomic events in this instability model, such as a high-amplitude genomic event on chromosome 2. By SKY, this is a recurrent non-reciprocal translocation involving chromosome 2 (band A3) with different partner chromosomes (Supplementary Fig. 3). By array-CGH, the CNAs in 4 independent TKO tumours shared a common boundary close to the 3' region of the *Notch1* gene, with 2 additional tumours harbouring *Notch1* focal amplifications (Supplementary Fig. 3; data not shown). NOTCH1 activation by carboxy-terminal structure alteration and point mutations is a signature event of human T-ALL^{3,26,27}. Although the murine genomic rearrangements differ from NOTCH1 translocations in human T-ALL²⁷, their common shared boundary involving *Notch1* suggested potential relevance to the TKO tumours. Thus, we performed *Notch1* re-sequencing in several TKO lymphomas lacking *Notch1* genomic rearrangement and uncovered truncating insertion/deletion mutations and non-conservative amino acid substitutions in the *Notch1* PEST and heterodimerization domains, as well as broader deletions within exon 34 encoding the PEST domain (Supplementary Fig. 4a; Supplementary Table 1). This mutation spectrum is analogous to that observed in human T-ALL, because the PEST and heterodimerization domains are two hot spots of NOTCH1 mutation (Supplementary Fig. 4a, see below)³. Biochemically, these mutations promote activation of mouse Notch1 as shown by higher levels of both full-length and the active cleaved form (V1744)²⁸ of Notch1 proteins (Supplementary Fig. 4b). Transcriptome profiling further showed upregulation of several Notch1 transcriptional targets including *Ptcra*, *Hes1*, *Dtx1* and *Cd3e*, which correlated well with messenger RNA levels of *Notch1*²⁶ (Supplementary Fig. 4c).

The observation of physiological deletion of *Tcr* loci and a human-like pattern of *Notch1* genomic and mutational events in TKO tumours prompted the assessment of the extent to which other CNAs emerging in TKO lymphomas mirrored those seen in human T-ALL. To this end, we first defined the minimal common regions

(MCRs, regions overlapping in more than one tumour as defined in Methods) in the TKO genome using an established algorithm with criteria of CNA width ≤ 10 Mb (megabases) and amplitude > 0.75 (\log_2 scale), yielding 160 MCRs with average sizes of 2.12 Mb (0.15–9.82 Mb) and 2.33 Mb (0.77–9.6 Mb) for amplifications and deletions, respectively (Supplementary Table 3). This frequency of genomic alterations is comparable to most human cancer genomes (for example, see below) and significantly above the typical 20 to 40 events detected in most genetically engineered 'genome-stable' murine tumour models^{8,10,11,29}. Next, by orthologue mapping of genes resident within the MCRs of CNAs, we compared the TKO MCRs with similarly defined MCRs in human T-ALL to identify syntenic overlap. Here, 18 of the 160 MCRs (11%) were found to overlap across species (Table 1); the extent to which overlap occurred was significantly greater than that expected by chance alone ($P = 0.001$ and 0.004 for deletions and amplifications, respectively). Moreover, these syntenic MCRs included several genes already implicated in T-ALL biology, such as *Crebbp*, *Ikaros* (also known as *Ikzf1*) and *Abli* (refs 30–32). These data support the relevance of murine models to human cancer biology and their potential use for human cancer gene discovery through comparative oncogenomics.

Frequent *Fbxw7* inactivation in T-ALL. A few TKO tumours with minimal Notch1 expression exhibited elevated *Notch4* or *Jagged1* (Notch ligand) mRNA levels (data not shown), prompting a detailed examination of the genomic and expression status of components in the Notch pathway. Indeed, a syntenic MCR encompassing the *Fbxw7* gene (MCR no. 18, Table 1; Fig. 2a) was observed across species. Although extremely focal in humans (Fig. 2a), the syntenic overlap made it unlikely that such deletion events represented copy number polymorphisms. *FBXW7* re-sequencing in a cohort of human T-ALL clinical specimens ($n = 38$) and cell lines ($n = 23$) (Supplementary Tables 2a, c and 4) revealed that *FBXW7* was mutated or deleted in 11/23 of the cell lines (48%) and 11/38 of the clinical samples (29%), making this one of the most commonly mutated genes in human T-ALL (Supplementary Tables 4 and 5). Consistent with reduced expression of *Fbxw7* relative to non-neoplastic thymus in 19 of the 24 TKO lymphomas (Fig. 2b), these *FBXW7* mutations in human T-ALL were predominantly mis-sense mutations, and particularly clustered in evolutionarily conserved arginine residues of the third and fourth WD40 domains involved in target binding³³ (Fig. 2c).

Moreover, re-sequencing of *FBXW7* in matched normal bone marrows from several patients in complete remission showed that the two most common mutations observed (R465, R479) were acquired somatically (data not shown). Additional mutations are likely to be somatic because the majority have been reported as somatic mutations in other tumour types (<http://www.sanger.ac.uk/genetics/CGP/cosmic/>) and none were present in public single nucleotide polymorphism databases. Finally, 19 of 21 mutations were heterozygous, consistent with reports that *Fbxw7* acts as a haplo-insufficient tumour suppressor gene³⁴.

FBXW7 is a component of the E3 ubiquitin ligase responsible for binding the NOTCH1 PEST domain, leading to ubiquitination and proteasome degradation³⁵. PEST domain mutations in human T-ALL prolong the half-life of intracellular NOTCH1, indicating that *FBXW7* loss may cause similar phenotypic effects. To address this, we characterized the cell lines and clinical samples for *NOTCH1* mutations (Supplementary Tables 2a, 2c, 4 and 5). Interestingly, there was no association between known functional mutations of *NOTCH1* (N-terminal (HD-N) and C-terminal (HD-C) heterodimerization domains and PEST domains) and *FBXW7* mutations ($P = 0.16$). However, among samples with *NOTCH1* mutations, *FBXW7* mutations were found less frequently in samples with a mutated PEST domain (4/19; 21%) than samples with mutations of only the HD-N or HD-C domain (13/20; 65%; $P = 0.009$). This is consistent with the hypothesis that mutations of *FBXW7* and the PEST domain of *NOTCH1* target the same degradation pathway, and little selective advantage accrues to the majority of tumours from mutating both components. On the other hand, the lack of *NOTCH1* and *FBXW7* mutation mutual exclusivity suggests that *FBXW7* affects other pathways in addition to NOTCH (see discussion).

Frequent *Pten* inactivation in mouse and human T-cell malignancy. Focal deletion on chromosome 19, centring on *Pten*, was among the most common genomic events in TKO lymphomas (Table 1; Fig. 1f). Array-CGH, coupled with real-time genomic PCR, documented homozygous deletions of *Pten* in 15/35 (43%) TKO lymphomas (Fig. 3; Supplementary Fig. 5). *PTEN* is a well-known tumour suppressor³⁶ and the inactivation of the homologue in the murine thymus is known to generate T-cell tumours³⁷. Correspondingly, array-CGH confirmed that 4 out of 26 human T-ALL samples had *PTEN* locus rearrangements. Additionally, re-sequencing of the 61 T-ALL cell lines and clinical specimens (Supplementary Table 2)

Table 1 | Synteny mapping between murine TKO lymphoma and human T-ALL MCRs

MCR no.	Cytoband	Start	Mouse TKO				Rec	Cancer genes or candidates		Human T-ALL			
			End	Size (bp)	Peak ratio	Chr		Start	End	Size (bp)	Peak ratio		
Amplification													
1	4E2	153,362,787	154,677,539	1,314,752	0.88	13	<i>Dvl1</i> ; <i>Ccnl2</i> ; <i>Aurkaip1</i>	1	1,286,939	1536335	249,396	1.11	
2	10A3	18,124,375	22,105,516	3,981,141	1.91	11	<i>Myb</i> ; <i>Ahi1</i>	6	135,471,648	135829074	357,426	1.07	
3	16C4	91,250,715	97,408,345	6,157,630	1.38	21	<i>Runx1</i> ; <i>Ets2</i> ; <i>Tmprss2</i> ; <i>Ripk4</i> ; <i>Erg</i>	21	40,837,575	42285661	1,448,086	0.95	
4	5G2	136,128,574	138,413,308	2,284,734	0.87	14	<i>Gnb2</i> ; <i>Perq1</i>	7	99,901,102	99949527	48,425	1.09	
5	4A1	5,601,642	13,568,807	7,967,165	1.00	11	<i>Tox</i>	8	59,880,732	60101149	220,417	0.82	
6	2B	29,315,580	31,992,174	2,676,594	1.78	7	<i>Set</i> ; <i>Fnbp1</i> ; <i>Abli</i> ; <i>Nup214</i>	9	130,710,910	131134550	423,640	2.06	
Deletion													
7	11B3–B4	68,759,068	72,041,187	3,282,119	–0.93	4	<i>Trp53</i> ; <i>Bcl6b</i>	17	6,494,426	7,767,821	1,273,395	–0.76	
8	3H4	155,474,073	158,861,389	3,387,316	–0.75	3	<i>Negr1</i>	1	71,919,083	72,444,137	525,054	–0.92	
9	15B3.1	33,212,025	41,060,793	7,848,768	–0.93	2	<i>BaalC</i> ; <i>Fzd6</i>	8	104,310,865	104,499,581	188,716	–0.93	
10	16A1	3,264,231	10,275,117	7,010,886	–0.97	21	<i>Crebbp</i> ; <i>Ciita</i>	16	3,195,168	11,549,999	8,354,832	–1.09	
11	19C3–D2	46,457,272	56,116,765	9,659,493	–0.77	8	<i>Mxi1</i>	10	111,672,720	112,043,485	370,765	–0.90	
12	4E2	150,778,332	154,677,539	3,899,207	–0.83	2	<i>Hes3</i> ; <i>Rpl22</i> ; <i>Chd5</i>	1	5,983,967	6,318,619.5	334,652	–0.85	
13	11A1	8,844,892	12,372,703	3,527,811	–3.73	14	<i>Ikaros</i>	7	49,539,939	50,229,252.5	689,313	–0.75	
14	12F2	111,667,310	115,272,402	3,605,092	–1.43	9	<i>Ptprn2</i>	7	156,125,925	158,194,699	2,068,774	–0.84	
15	6B1	41,191,601	41,690,238	498,637	–5.48	28	<i>Terb</i>	7	141,785,426	142,078,458	293,032	–3.07	
16	19A	11,295,986	15,610,191	4,314,205	–0.77	4	<i>Gnaq</i>	9	77,572,992	77,916,022	343,030	–0.76	
17	19C1	31,573,449	32,118,682	545,233	–4.48	13	<i>Pten</i>	10	89,594,719	90,035,234	440,515	–3.30	
18	3E3–F1	79,297,034	87,003,791	7,706,757	–0.93	2	<i>Fbxw7</i>	4	153,078,068	154,979,435	1,901,367	–1.74	

Each murine TKO MCR with syntenic overlap with an MCR in the human T-ALL data set is listed—separated by amplification and deletion—along with its chromosomal location (Cytoband/Chr) and base number (Start and End, in base pairs). The minimal size of each MCR is indicated in base pairs (bp). Peak ratio refers to the maximal \log_2 array-CGH ratio for each MCR. Rec refers to the number of tumours in which the MCR was defined.

uncovered inactivating *PTEN* mutations in 9 cases, none of which was found in public SNP databases. Each is predicted to cause protein truncation and is observed in other cancers³⁶ but shows no clear correlation with *NOTCH1* mutations (Supplementary Tables 4 and 5). *PTEN* mutations were more frequent in cell lines (7/23; 30.4%) than in clinical specimens (2/38; 5.2%) (Supplementary Table 4). Because these clinical specimens were newly diagnosed cases, whereas the cell lines were mostly established from relapses, this difference in mutation frequency may suggest that *PTEN* inactivation is a later event associated with progression, among other possibilities.

Northern and western blot analyses and transcriptome profiling of the TKO and human T-ALL samples revealed a broader collection of tumours with low to undetectable *PTEN* expression (Fig. 3b, data not shown) with elevated phospho-AKT. Moreover, AKT activation may have been driven by focal Akt1 amplification and *Tsc1* loss in two TKO samples (Fig. 3c; data not shown). Lastly, the biological significance of *Pten* status in TKO lymphoma is supported by their sensitivity to Akt inhibition in a *Pten*-dependent manner (Supplementary Fig. 6) in response to triciribine, a drug known to block Akt phosphorylation and inhibit cells dependent on the Akt pathway³⁸.

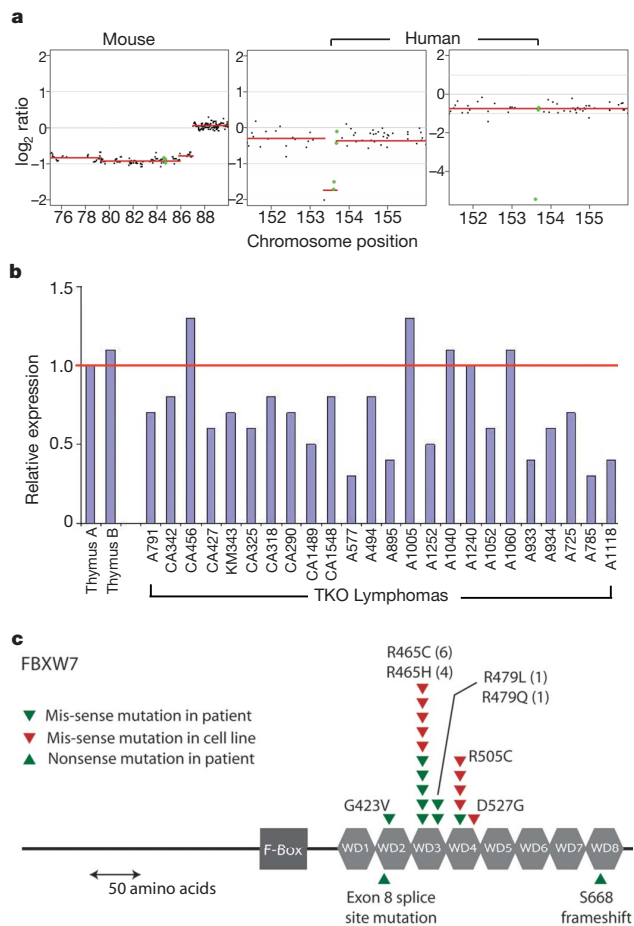


Figure 2 | *FBXW7* alterations are common in human T-ALL and conserved in the murine TKO tumours. **a**, \log_2 ratio of array-CGH plots showing conserved deletion of *FBXW7* in both mouse TKO and human T-ALL cell lines; *FBXW7* is indicated in green. The y axis shows \log_2 of copy number ratio (normal, $\log_2 = 0$); amplifications are above and deletions are below this axis; x axis, chromosome position, in Mbp. **b**, Relative expression level (by real-time quantitative PCR) of mouse *Fbxw7* mRNA in murine TKO tumours, with expression in normal thymus (thymus A) set at 1; an independent normal thymus sample (thymus B) was run for comparison. **c**, Location of *FBXW7* mutations in a panel of human T-ALL patients and cell lines. Each marker represents an individual cell line/patient.

Broad comparison of the TKO genome with diverse human cancers.

Although cross-species comparison showed numerous concordant lesions in cancers of T-cell origin, the fact that this instability model is driven by mechanisms of fundamental relevance (telomere dysfunction and Trp53 mutation) to many cancer types suggested potentially broader relevance to other human cancers. A case in point is the *PTEN* example above; *PTEN* is a tumour suppressor for multiple cancers³⁶. We therefore extended the cross-species comparative genomic analyses to 6 other human cancer types ($n = 421$) of haematopoietic, mesenchymal and epithelial origins, including multiple myeloma ($n = 67$)³⁹, glioblastoma ($n = 38$) (unpublished) and melanoma ($n = 123$) (unpublished), as well as pancreatic ($n = 30$) (unpublished), lung ($n = 63$)⁴⁰ and colon adenocarcinomas ($n = 74$) (unpublished).

Compared to similarly defined MCR lists (that is, MCR width ≤ 10 Mb; Fig. 4a) of each of these cancer types, we found that 102 (61 amplifications, 41 deletions) of 160 MCRs (64%) in the TKO genomes matched with at least 1 MCR in 1 human array-CGH data set, with strong statistical significance attesting to non-randomness of the overlap (Fig. 4a). Confidence in the relevance of these syntenic events was bolstered by the observation that more than half of these syntenic MCRs (38 of 61 amplifications or 62%; 22 of 41 deletions or

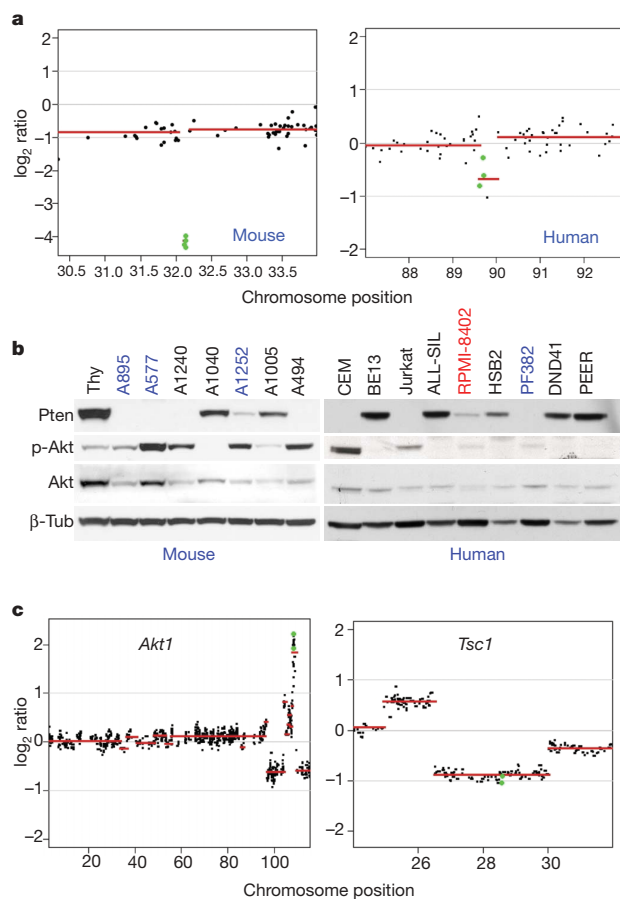


Figure 3 | Conservation of *PTEN* genetic alterations in human and mouse T-ALLs. **a**, Array-CGH plots showing conserved deletion of *PTEN* in both mouse TKO and human T-ALL cell lines; *PTEN* indicated in green. The y axis shows \log_2 ratio of copy number (normal, $\log_2 = 0$); amplifications are above and deletions are below the red axis. **b**, Western blotting for *PTEN*, phospho-Akt, Akt and tubulin (loading control) in a panel of murine TKO and human T-ALL cell lines. BE13 and PEER are synonymous lines. Samples in red harbour confirmed sequence mutations; samples in blue harbour aCGH-detected deletions. **c**, CNAs affecting other members of the *Pten-Akt* axis are shown as \log_2 ratio plots for murine TKO tumours. The location of each gene (*Akt1/Tsc1*) is shown in green.

53%) overlapped with MCRs recurrent in two or more human tumour types (Fig. 4b). Moreover, a significant proportion of the TKO MCRs were evolutionarily conserved in human tumours of non-haematopoietic origin (Fig. 4c). Among the 61 amplifications with syntenic hits, 58 of them (95%) were observed in solid tumours, whereas the remaining 3 were uniquely found in myeloma (Fig. 4c). Similarly, 33 of 41 (80%) syntenic deletions were present in solid tumours (Fig. 4c). Among these are *Trp53*, deleted in 5 of 7 human cancer types, and *Myc* amplifications in 6 human cancers. This substantial overlap with diverse human cancers was unexpected.

Next, to provide an additional level of validation for these TKO genomic events, we determined whether these syntenic MCRs targeted known cancer genes. Mouse homologues were found for 237 of 363 genes listed on the Cancer Gene Census⁴¹, and of these, 24 were found within the 104 syntenic MCRs (Supplementary Table 6). These included 17 oncogenes in amplifications and 7 tumour suppressor genes in deletions. However, the majority of these syntenic MCRs do not contain known cancer genes, raising the strong possibility that re-sequencing that is focused on resident genes of syntenic MCRs may

provide a high-yield strategy to identify somatic mutations in human cancers, a thesis supported by the *FBXW7* and *PTEN* examples.

Discussion

We describe here the characterization of a mouse model of T-cell lymphoma engineered with telomere and checkpoint defects. In these unstable murine tumours, cytogenetic and copy number analyses reveal a level of genome complexity comparable to that of human solid tumours. The presence of rampant genome instability, and absence of an engineered dominantly acting oncogene, created a model system in which biological selection pressures drive acquired genomic events with potential relevance to human T-cell malignancy and/or cancer in general. In this model, murine cancers acquire widespread recurrent clonal CNAs targeting loci syntenic to alterations present in a human T-ALL as well as a large collection of diverse haematopoietic, mesenchymal and epithelial cancers. The relevance of these non-random syntenic events is supported on several levels, including the presence of syntenic MCRs in more than one human cancer type; the identification of MCRs harbouring known cancer genes; and the identification of somatic mutations in genes within conserved MCRs (*FBXW7* and *PTEN*).

Evolutionarily conserved genomic deletions targeting the *FBXW7* and *PTEN* loci motivated re-sequencing of them in human and murine T-ALL samples, revealing frequent mutations. *FBXW7* mutation has been described in about 5% of colorectal and ovarian cancers^{42–44}, although its involvement in T-ALL has not been reported previously. As a key component of the E3 ubiquitin ligase that ubiquitinates NOTCH1, loss or mutation of *FBXW7* is expected to be functionally equivalent to PEST domain mutation of *NOTCH1*, prolonging NOTCH1 half-life³⁵. Indeed, a statistically significant anti-correlation is observed between presence of PEST domain mutations in *NOTCH1* and presence of *FBXW7* mutation in human T-ALL samples. However, the fact that several samples with *FBXW7* mutations have wild-type *NOTCH1* (5/22) strongly implies that other pathways may be affected by *FBXW7* mutations in some cancers. Indeed, *FBXW7* is known to promote degradation of other proteins implicated in lymphoma biology such as Aurora A (also known as AURKA), c-Jun (JUN), Cyclin E (CCNE1) and C-myc (MYC)^{34,35}, the latter of which is also a transcriptional target of NOTCH signalling⁴⁵.

In summary, the compelling synteny between TKO tumours and several human cancers of diverse origins demonstrates that engineered chromosomal instability in the mouse can engender genomic alterations similar to those observed in complex human oncogenomes, providing evidence that murine and human tumours experience common biological processes driven by the orthologous genetic events. These results provide support for the use of such murine models as a guidepost to focus and prioritize re-sequencing efforts in human cancer because cross-species synteny serves as a measure of validation by virtue of the evolutionary conservation and use of different genetic mechanisms (that is, mutation and copy number) involved. Furthermore, the mouse can facilitate the differentiation between somatic CNAs and copy number polymorphisms owing to the fragmentation of syntenic regions in the mouse and human genomes. We conclude that genomically unstable mouse cancer models represent a valuable resource for mining complex human cancer genomes.

METHODS SUMMARY

Terc Atm- and *Terc Trp53*-deficient mice described previously^{21,46} were interbred, maintained in pathogen-free facilities and followed for lymphoma development. Resultant TKO lymphomas were harvested from moribund animals and metaphase preparations of primary cultures were used for SKY profiling. DNA and RNA were extracted from the murine TKO tumours as well as from human cancer cell lines and tumours for performing array-CGH and transcriptome profiling, respectively. MCRs of 10 Mb or smaller were defined by described algorithms^{39,47} for murine lymphomas and each of the 6 different human cancer types. Syntenic overlap was determined based on orthologue mapping of MCR resident genes and statistic significance of the overlap calculated by permutation. Known cancer genes were as defined by the Cancer Gene Census⁴¹ (<http://www.sanger.ac.uk/>)

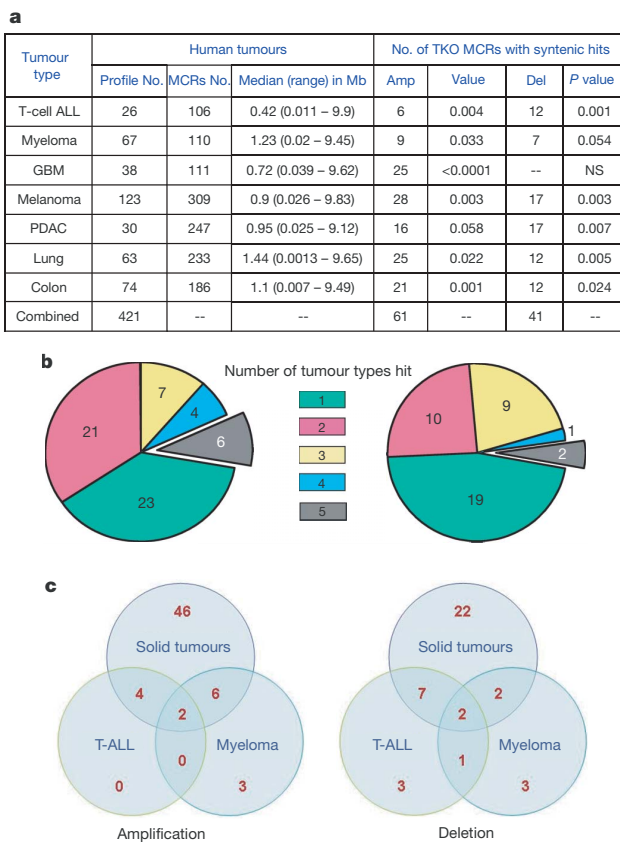


Figure 4 | Substantial overlap between genomic alterations of murine TKO lymphomas and human tumours of diverse origins. **a**, Characteristics of MCRs from human array-CGH profiles from the indicated tumour types are listed on the left portion of the panel. PDAC, pancreatic adenocarcinoma. The number of TKO MCRs (Amp, amplifications; Del, deletions) with syntenic overlap with the corresponding human CGH data set is indicated on the right side of the panel (*P* value is based on 10,000 permutations). **b**, Pie-chart showing numbers of TKO MCRs (indicated within each segment) with syntenic overlap identified in one or multiple human tumour types (indicated by different colours of the segments); left panel, amplifications; right panel, deletions. **c**, Venn diagram representation of overlap between murine TKO MCRs and MCRs from human cancers of T-ALL, multiple myeloma, or solid tumours (encompassing glioblastoma, melanoma, and pancreatic, lung and colon adenocarcinoma).

genetics/CGP/Census). Gene mutation status was established by denaturing high-performance liquid chromatography as previously published⁴⁸, and by bidirectional sequencing. All eight array-CGH data sets used in this study are available on the GEO website under the accession number GSE7615.

Full Methods and any associated references are available in the online version of the paper at www.nature.com/nature.

Received 26 March; accepted 30 April 2007.

Published online 21 May 2007.

- Pinkel, D. & Albertson, D. G. Array comparative genomic hybridization and its applications in cancer. *Nature Genet.* **37** (Suppl) S11–S17 (2005).
- Davies, H. *et al.* Mutations of the *BRAF* gene in human cancer. *Nature* **417**, 949–954 (2002).
- Weng, A. P. *et al.* Activating mutations of NOTCH1 in human T cell acute lymphoblastic leukemia. *Science* **306**, 269–271 (2004).
- Sweet-Cordero, A. *et al.* An oncogenic *KRAS2* expression signature identified by cross-species gene-expression analysis. *Nature Genet.* **37**, 48–55 (2005).
- Hodgson, G. *et al.* Genome scanning with array CGH delineates regional alterations in mouse islet carcinomas. *Nature Genet.* **29**, 459–464 (2001).
- O'Hagan, R. C. *et al.* Telomere dysfunction provokes regional amplification and deletion in cancer genomes. *Cancer Cell* **2**, 149–155 (2002).
- Casanovas, O., Hager, J. H., Chun, M. G. & Hanahan, D. Incomplete inhibition of the Rb tumor suppressor pathway in the context of inactivated p53 is sufficient for pancreatic islet tumorigenesis. *Oncogene* **24**, 6597–6604 (2005).
- Bardeesy, N. *et al.* Both p16^{Ink4a} and the p19^{Arf}-p53 pathway constrain progression of pancreatic adenocarcinoma in the mouse. *Proc. Natl Acad. Sci. USA* **103**, 5947–5952 (2006).
- Pelham, R. J. *et al.* Identification of alterations in DNA copy number in host stromal cells during tumor progression. *Proc. Natl Acad. Sci. USA* **103**, 19848–19853 (2006).
- Kim, M. *et al.* Comparative oncogenomics identifies *NEDD9* as a melanoma metastasis gene. *Cell* **125**, 1269–1281 (2006).
- Zender, L. *et al.* Identification and validation of oncogenes in liver cancer using an integrative oncogenomic approach. *Cell* **125**, 1253–1267 (2006).
- O'Neil, J. *et al.* Activating *Notch1* mutations in mouse models of T-ALL. *Blood* **107**, 781–785 (2005).
- Sweet-Cordero, A. *et al.* Comparison of gene expression and DNA copy number changes in a murine model of lung cancer. *Genes Chromosom. Cancer* **45**, 338–348 (2006).
- Artandi, S. E. *et al.* Telomere dysfunction promotes non-reciprocal translocations and epithelial cancers in mice. *Nature* **406**, 641–645 (2000).
- Zhu, C. *et al.* Unrepaired DNA breaks in p53-deficient cells lead to oncogenic gene amplification subsequent to translocations. *Cell* **109**, 811–821 (2002).
- Lang, G. A. *et al.* Gain of function of a p53 hot spot mutation in a mouse model of Li-Fraumeni syndrome. *Cell* **119**, 861–872 (2004).
- Olive, K. P. *et al.* Mutant p53 gain of function in two mouse models of Li-Fraumeni syndrome. *Cell* **119**, 847–860 (2004).
- Hingorani, S. R. *et al.* Trp53R172H and KrasG12D cooperate to promote chromosomal instability and widely metastatic pancreatic ductal adenocarcinoma in mice. *Cancer Cell* **7**, 469–483 (2005).
- Qi, L., Strong, M. A., Karim, B. O., Huso, D. L. & Greider, C. W. Telomere fusion to chromosome breaks reduces oncogenic translocations and tumour formation. *Nature Cell Biol.* **7**, 706–711 (2005).
- Qi, L. *et al.* Short telomeres and ataxia-telangiectasia mutated deficiency cooperatively increase telomere dysfunction and suppress tumorigenesis. *Cancer Res.* **63**, 8188–8196 (2003).
- Wong, K. K. *et al.* Telomere dysfunction and Atm deficiency compromises organ homeostasis and accelerates ageing. *Nature* **421**, 643–648 (2003).
- Shiloh, Y. & Kastan, M. B. ATM: genome stability, neuronal development, and cancer cross paths. *Adv. Cancer Res.* **83**, 209–254 (2001).
- Liyanage, M. *et al.* Abnormal rearrangement within the α/δ T-cell receptor locus in lymphomas from *Atm*-deficient mice. *Blood* **96**, 1940–1946 (2000).
- Rudolph, K. L., Millard, M., Bosenberg, M. W. & DePinho, R. A. Telomere dysfunction and evolution of intestinal carcinoma in mice and humans. *Nature Genet.* **28**, 155–159 (2001).
- Windle, B., Draper, B. W., Yin, Y. X., O'Gorman, S. & Wahl, G. M. A central role for chromosome breakage in gene amplification, deletion formation, and amplicon integration. *Genes Dev.* **5**, 160–174 (1991).
- Radtke, F., Wilson, A., Mancini, S. J. & MacDonald, H. R. Notch regulation of lymphocyte development and function. *Nature Immunol.* **5**, 247–253 (2004).
- Ellisen, L. W. *et al.* *TAN-1*, the human homolog of the *Drosophila Notch* gene, is broken by chromosomal translocations in T lymphoblastic neoplasms. *Cell* **66**, 649–661 (1991).
- Schroeter, E. H., Kisslinger, J. A. & Kopan, R. Notch-1 signalling requires ligand-induced proteolytic release of intracellular domain. *Nature* **393**, 382–386 (1998).
- O'Hagan, R. C. *et al.* Array comparative genome hybridization for tumor classification and gene discovery in mouse models of malignant melanoma. *Cancer Res.* **63**, 5352–5356 (2003).
- Shigeno, K. *et al.* Disease-related potential of mutations in transcriptional cofactors CREB-binding protein and p300 in leukemias. *Cancer Lett.* **213**, 11–20 (2004).
- Winandy, S., Wu, P. & Georgopoulos, K. A dominant mutation in the *Ikaros* gene leads to rapid development of leukemia and lymphoma. *Cell* **83**, 289–299 (1995).
- Graux, C. *et al.* Fusion of NUP214 to ABL1 on amplified episomes in T-cell acute lymphoblastic leukemia. *Nature Genet.* **36**, 1084–1089 (2004).
- Orlicky, S., Tang, X., Willems, A., Tyers, M. & Sicheri, F. Structural basis for phosphodependent substrate selection and orientation by the SCFCdc4 ubiquitin ligase. *Cell* **112**, 243–256 (2003).
- Mao, J. H. *et al.* *Fbxw7/Cdc4* is a p53-dependent, haploinsufficient tumour suppressor gene. *Nature* **432**, 775–779 (2004).
- Minella, A. C. & Clurman, B. E. Mechanisms of tumor suppression by the SCFFbw7. *Cell Cycle* **4**, 1356–1359 (2005).
- Sansal, I. & Sellers, W. R. The biology and clinical relevance of the *PTEN* tumor suppressor pathway. *J. Clin. Oncol.* **22**, 2954–2963 (2004).
- Suzuki, A. *et al.* High cancer susceptibility and embryonic lethality associated with mutation of the *PTEN* tumor suppressor gene in mice. *Curr. Biol.* **8**, 1169–1178 (1998).
- Yang, L. *et al.* Akt/protein kinase B signaling inhibitor-2, a selective small molecule inhibitor of Akt signaling with antitumor activity in cancer cells overexpressing Akt. *Cancer Res.* **64**, 4394–4399 (2004).
- Carrasco, D. R. *et al.* High-resolution genomic profiles define distinct clinicopathogenetic subgroups of multiple myeloma patients. *Cancer Cell* **9**, 313–325 (2006).
- Tonon, G. *et al.* High-resolution genomic profiles of human lung cancer. *Proc. Natl Acad. Sci. USA* **102**, 9625–9630 (2005).
- Futreal, P. A. *et al.* A census of human cancer genes. *Nature Rev. Cancer* **4**, 177–183 (2004).
- Rajagopalan, H. *et al.* Inactivation of *hCDC4* can cause chromosomal instability. *Nature* **428**, 77–81 (2004).
- Kemp, Z. *et al.* *CDC4* mutations occur in a subset of colorectal cancers but are not predicted to cause loss of function and are not associated with chromosomal instability. *Cancer Res.* **65**, 11361–11366 (2005).
- Kwak, E. L. *et al.* Infrequent mutations of Archipelago (*hAGO*, *hCDC4*, *Fbw7*) in primary ovarian cancer. *Gynecol. Oncol.* **98**, 124–128 (2005).
- Sharma, V. M., Draheim, K. M. & Kelliher, M. A. The Notch1/c-Myc Pathway in T cell leukemia. *Cell cycle* **6**, 327–330 (2007).
- Chin, L. *et al.* p53 deficiency rescues the adverse effects of telomere loss and cooperates with telomere dysfunction to accelerate carcinogenesis. *Cell* **97**, 527–538 (1999).
- Aguirre, A. J. *et al.* High-resolution characterization of the pancreatic adenocarcinoma genome. *Proc. Natl Acad. Sci. USA* **101**, 9067–9072 (2004).
- Mansour, M. R., Linch, D. C., Foroni, L., Goldstone, A. H. & Gale, R. E. High incidence of Notch-1 mutations in adult patients with T-cell acute lymphoblastic leukemia. *Leukemia* **20**, 537–539 (2006).
- Olshen, A. B., Venkatraman, E. S., Lucito, R. & Wigler, M. Circular binary segmentation for the analysis of array-based DNA copy number data. *Biostatistics* **5**, 557–572 (2004).
- Davies, H. *et al.* Somatic mutations of the protein kinase gene family in human lung cancer. *Cancer Res.* **65**, 7591–7595 (2005).

Supplementary Information is linked to the online version of the paper at www.nature.com/nature.

Acknowledgements We thank Y. Zhang, A. Yu and K. Marmon for excellent mouse husbandry and care, and C. Greenman and E. Pleasance for helpful discussion on statistical analyses. R.S.M. was supported by the Damon Runyon Cancer Research Foundation. P.J.C. was supported by the Kay Kendall Leukaemia Fund, and B.C. is supported by a grant from GlaxoSmithKline. K.K.W. was supported by an NIH award. M.R.S. and P.A.F. are supported by the Wellcome Trust. L.C. and R.A.D. are supported by NIH grants, LeBow Fund to Cure Myeloma, the Chris Elliot Foundation, and the Center for Applied Cancer Science of the Belfer Institute for Innovative Cancer Science. R.A.D. is an Ellison Foundation for Medical Research Senior Scholar and an American Cancer Society Research Professor.

Author Contributions R.S.M., B.C., P.J.C. and B.F. performed the experiments and contributed equally as first authors. M.R.S., L.C., P.A.F. and R.A.D. supervised experiments and contributed equally as senior authors. R.S.M. and R.A.D. generated and characterized the instability mouse model. B.F. and L.C. conducted the oncogenomic analyses. B.C., P.J.C., M.R.S. and P.A.F. provided the re-sequencing analyses. A.P., J.O., A.G., E.I., I.P., E.L., V.M., S.J., K.M., S.Z., S.E., C.S., G.H., C.B., E.S.M., R.W., O.K., C.N., M.M. and V.D. performed experiments. A.G., L.F., A.K.F., A.H.G., J.M.R. and A.T.L. contributed patient samples and clinical data. K.K.W., J.A. and A.T.L. coordinated experiments. Y.A.W. contributed to the writing of the manuscript.

Author Information All microarray data are available at the Gene Expression Array Omnibus website (<http://www.ncbi.nlm.nih.gov/geo/>) under accession number GSE7615. Reprints and permissions information is available at www.nature.com/reprints. The authors declare no competing financial interests. Correspondence and requests for materials should be addressed to R.A.D. (ron_depinho@dfci.harvard.edu).

METHODS

Mice. *Terc Atm* and *Terc Trp53* deficient mice have been described previously^{21,46}. Mice were interbred and maintained in pathogen-free conditions at Taconic Farms and Dana-Farber Cancer Institute, monitored for signs of ill-health every other day, and euthanized and necropsied when moribund. Mice found dead were necropsied specifically for signs of lymphoma. All manipulations were performed with IACUC approval.

Tumour characterization and sample preparation. Tumours harvested from TKO mice were partitioned for DNA, RNA and protein extraction, for histology (Brigham and Women's Hospital), and for *in vitro* culture. Tumour cells were cultured in RPMI with 50 μ M β -mercaptoethanol, 10% CosmicCalf serum (HyClone), 0.5 ng ml⁻¹ IL-2 (Peprotech), and 4 ng ml⁻¹ IL-7 (Peprotech). For FACS analysis, cells were immunostained with CD4, CD8, CD3 and B220/CD45R antibodies (eBioscience) and scanned on a FACScalibur (BD Biosciences). For SKY analyses, metaphases were obtained from colcemid-treated cells incubated in 105 mM KCl hypotonic buffer for 15 min before fixation in 3:1 methanol-acetic acid. Spectral karyotyping was done using the SkyPaint Kit and SkyView analytical software (Applied Spectral Imaging) according to manufacturer's protocols. Chromosome aberrations were defined in accordance with the Committee on Standard Genetic Nomenclature for Mice.

DNA was prepared with the PureGene kit (Gentra Systems). Real-time PCR was performed with a Quantitect SYBR green kit (Qiagen) using 2 ng DNA from each tumour run in triplicate and the primers listed in Supplementary Table 7, on Applied Biosystems or Stratagene MX3000 real-time thermocyclers; copy number average of two runs was calculated using the standard curve method. RNA was extracted with Trizol (Invitrogen) according to the manufacturer's instructions, then digested with RQ1 DNase (Promega) and purified through RNA purification columns (Gentra). Reverse transcription was performed with oligo dT primers with the Oligoscript kit (Qiagen). Protein lysates were prepared by dis-aggregation in lysis buffer (Cell Signaling Technology) followed by bath sonication for 30 s. Clarified lysates were quantified with BioRad protein assay according to manufacturer's instructions, separated on 4–12% NuPage gels (Invitrogen), and transferred to PVDF membranes (Immobilon). Immunoblotting was performed with antibodies against PTEN, AKT, phospho-AKT, NOTCH1, activated NOTCH1 Val1744 (all from Cell Signaling Technology), and tubulin (Sigma) and developed with HRP-labelled secondary antibodies (Pierce) and enhanced chemiluminescent substrate.

Human T-ALL samples and cell lines. T-ALL cell lines were subjected to both array-CGH and/or re-sequencing, as indicated (Supplementary Table 2a).

Two cohorts of clinical human T-ALL samples were used. A cohort of 8 clinical samples (Supplementary Table 2b), subjected to array-CGH, was obtained with informed consent and IRB approval at time of diagnosis from paediatric patients with T-ALL treated on the Dana-Farber Cancer Institute study 00-001. An independent series of 38 clinical specimens (Supplementary Table 2c), used for re-sequencing, was collected at presentation from 8 children and adolescents diagnosed at the Royal Free Hospital, London, and 30 adult patients enrolled in the MRC UKALL-XII trial. Informed consent was obtained from the patients (if over 18 yr of age) or their guardians (if under 18 yr) with Ethics Committee approval.

Array-CGH profiling and analyses. Array-CGH: genomic DNA processing, labelling and hybridization to Agilent CGH 60-mer oligo arrays were performed as per the manufacturer's protocol (<http://www.home.agilent.com/agilent/home.jsp>). Murine tumours were profiled against matched normal DNA or, when not available, pooled DNA of matched strain background. Labelled DNAs were hybridized onto 44K or 244K microarrays for mouse, and 22K, 44K, or 244K microarrays for human (detailed feature information for each at www.agilent.com). Profiles generated on 244K arrays were extracted for the same 42K probes on the 44K microarrays to allow combination of profiles generated on the different platforms. Fluorescence ratios of scanned images were normalized and averaged from two pairs (dye swap), and copy number profile was generated by Circular Binary Segmentation, which determines significance of change points in raw data through permutation⁴⁹.

Definition of MCRs: minimal common region (MCR) definition was described previously^{39,47}. Briefly, a 'segmented' data set was determined from uniform copy number segment boundaries, then replacing raw log₂ ratio for each probe by the mean log₂ ratio of the segment containing the probe. Thresholds for copy number alterations were set at log₂ = ± 0.4 and ± 0.6 for 22K and 44K arrays, respectively, with higher thresholds for 44K profiles adjusting for differences in signal:noise detection. MCRs required at least one sample to show an extreme CNA event, (log₂ ratio $\geq \pm 0.60$ and ± 0.75 for 22K and 44K profiles, respectively, and the width less than 10 Mb).

Homologue mapping: genes within mouse TKO MCRs were used to obtain their human homologue on the basis of the NCBI homologue website (<http://www.ncbi.nlm.nih.gov/entrez/query.fcgi?db=homologue>). For cancer gene

mapping, mouse homologues were obtained on the basis of the Sanger Cancer Gene Census⁴¹ (<http://www.sanger.ac.uk/genetics/CGP/Census>).

Permutation testing: permutation testing was conducted for statistical significance of MCR overlap by randomly generating a simulated mouse genome containing the same number and sizes of MCRs in the corresponding chromosomes as the actual TKO genome; a similar set was created for each human cancer data set. The number of overlapping MCRs between mouse and each human genome was calculated and stored, and repeated 10,000 times independently for amplifications and deletions. The *P* value for significance of overlap for each was calculated by dividing the frequency of randomly achieved overlap by 10,000.

Mutation screening. Mutational status was established by denaturing high-performance liquid chromatography⁴⁸ and by bidirectional sequencing. Genomic DNA was extracted using the Qiagen genomic purification kit. PCR amplification and direct sequencing were done as previously described³⁹. Sequence traces were analysed using manual and software-based analyses. All variants were confirmed by bidirectional sequencing of a second independently amplified PCR product.

Expression profiling. Biotinylated target complementary RNA was generated from total sample RNA and hybridized to 44K Mouse Development Oligo Microarrays (Agilent) against normal control murine thymus RNA according to the manufacturer's protocols. Expression values for each gene were mapped to genomic positions on the basis of National Center for Biotechnology Information Build 34 of the mouse genome.

Drug sensitivity. Cells (20,000) were plated in triplicate in 96-well format and incubated in media with varying doses of tricitriline (BioMol) or vehicle (DMSO; Sigma) for 2 days, after which growth was quantified using the AqueousOne Cell Titer System (Promega). Relative cell growth was plotted versus equivalent amount of DMSO alone as control, and 3–5 replicates were performed for each.